GENERATION OF TURBULENT INLET-BOUNDARY CONDITIONS USING POD-MODES

Peter S. Johansson, Helge I. Andersson
Department of Energy and Process Engineering
Norwegian University of Science and Technology
7491 Trondheim, Norway
peterj@mtf.ntnu.no, helge.i.andersson@mtf.ntnu.no

ABSTRACT

A very large-eddy simulation based on a small set, $\mathcal{S}$, of POD-modes of turbulent channel flow is performed in order to generate turbulent inlet-boundary conditions for a DNS of the same flow. On to the large-scale motion small-scale random POD-modes, not included in the set $\mathcal{S}$, are added in order to impose some energy in the high wave-number part of the spectrum. It is found that the normal Reynolds stresses and the energy spectra attain the same level as in fully developed channel flow approximately 5 channel heights downstream the inlet.

INTRODUCTION

Restriction of the computational domain to places of interest is essential to reduce simulation costs. The drawback of smaller domains is that they require better boundary conditions since the flow will have a shorter distance to develop. Steady laminar inflow boundary conditions are rather simple to prescribe, but turbulent boundary conditions are a completely different issue. It is generally not possible to let the turbulence develop from a laminar state at the boundary since this would require a large region, if not all, of the computational domain. The incoming turbulence at the boundary should have a correct mean value, fulfill the incompressibility constraint, have proper one- and two-point correlations and ultimately meet the momentum equation. This can be achieved by employing periodic (Kim et al., 1987) or quasi-periodic boundary conditions (Lygren and Andersson, 2001). Turbulence structures that leave the domain re-enter at the opposite side. Periodic boundary conditions severely limit the type of flow cases to be simulated. Statistical homogeneity, or at least statistical quasi-homogeneity, is needed in the directions for which periodic boundary conditions are used. This excludes most engineering flows in which the object under study usually will disarrange homogeneity. A way out of this is to perform a separate simulation (Manhart and Wengle, 1993) in order to produce fully developed inflow boundary conditions. The disadvantage is of course the cost of the extra simulation in which one is not interested. Our experience with channel flow simulations is that the time needed to arrive at a fully developed turbulent flow is comparable to the time needed to gather statistics. The efforts spent on producing realistic boundary conditions also prevent a wider application of LES for industrial problems.

The objective of this study is to investigate the possibility of producing inflow boundary conditions for DNS/LES by doing a very-large-eddy simulation (VLES) and superimpose random small-scale fluctuations on to the large-scale motion. The idea is that the large structures which make up an overwhelming part of the turbulent energy also constitute the dominant physics and should therefore be properly represented. If not, the mean flow will convect the structures far downstream of the inlet before they behave in a physically correct way. Random small-scales are added to have some energy in the high wave-number part of the spectrum. These low-energy structures are assumed to be of modest dynamical significance, and because of their shorter time-scale they will hopefully adjust themselves to give meaningful turbulence shortly downstream the inlet.

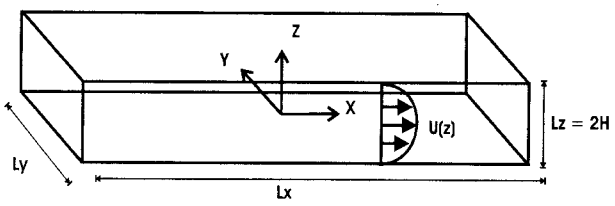

Figure 1: Sketch of the flow geometry with coordinate system.

FLOW GEOMETRY AND GOVERNING EQUATIONS

Plane channel flow is chosen as the test case for the generation of turbulent inlet-boundary conditions technique. The geometry is very simple (see figure 1), minimising the number of parameters. While being homogeneous in the spanwise and streamwise directions, the flow is strongly inhomogeneous in the wall-normal direction and holds the most important mechanisms and characteristics of self-sustaining turbulence.

The normalised Navier-Stokes equations describing the flow are

$$\frac{\partial \boldsymbol{u}}{\partial t} + \boldsymbol{u}\cdot\nabla\boldsymbol{u} = -\nabla p + \frac{1}{R_*}\nabla^2\boldsymbol{u} \qquad (1)$$

$$\nabla\cdot\boldsymbol{u} = 0 \qquad (2)$$

in which $\boldsymbol{u} = \boldsymbol{u}'/u_*$, $t = t'u_*/H$, $p = p'/(\rho u_*^2)$, $\boldsymbol{x} = \boldsymbol{x}'/H$ and the Reynolds number, $R_* = u_*H/\nu$. The prime indicates dimensional quantities, u_* is the friction velocity, H the half-channel height and ν the kinematic viscosity.

METHOD USED TO GENERATE INFLOW DATA

The inflow generation technique studied here is based on the proper orthogonal decomposition (POD) method (Lumley, 1967) and can be divided into five steps. The first step is a DNS of turbulent plane channel flow (which is the flow

we "cheaply" want to reproduce). For historical reasons the Reynolds number based on friction velocity (R_*) equal to 180 is selected. The second step is the POD of the same flow. Then comes "the very large-eddy simulation" (VLES) based on the POD-modes extracted in the previous step. The fourth stage consists of superposition of small-scale random motion not represented in the VLES on to the large-scale motion. Finally, the generated velocity field consisting of both random and deterministic motion is introduced on the inlet-boundary of a plane channel to verify that this can be a meaningful way of generating turbulent inflow boundary conditions.

DNS of Plane Channel Flow at R_*=180

The DNS is performed with the finite-volume code MGLET in order to establish a database from which the POD-modes can be extracted. The 4th-order compact scheme is used for spatial discretization, while the second-order explicit Adams-Bashforth scheme is used for time integration. The simulation box measures $4\pi H$, $4\pi H/3$ and $2H$ in $x-$, $y-$ and $z-$direction, respectively. The resolution is 128 x 128 x 128 grid-points. Equal spacing is used in the two homogeneous directions. In the normal direction the grid has a constant stretching of 2%. The first pressure point is placed at $z^+ = 0.7$. The database consists of 110 complete velocity fields dumped every 0.5 large-eddy-turn-over-time ($= H/u_*$) after reaching statistical steady state. The root-mean-square (rms) values of the Reynolds stresses and the mean velocity coincide with the reference simulation (Kim et al., 1987) (not shown here).

Proper Orthogonal Decomposition (POD)

Lumley (1967) proposed the proper orthogonal decomposition as an unbiased and therefore appropriate method to detect coherent structures in turbulent flows. These "structures" constitute a set of orthogonal basis functions which are optimal in respect to representing the energy of the velocity fields from which the POD-modes are derived. Other very favourable qualities of the POD-modes are that they fulfill the incompressibility constraint (Holmes et al., 1996) and the same boundary conditions as the velocity field.

In homogeneous directions Lumley (1967) showed that the POD-modes are the Fourier modes and in the case of plane channel flow only the wall-normal expansion of the POD-modes is a priori unknown. The eigenfunctions will thus be of the form

$$\varphi^q_{mn}(\boldsymbol{x}) = \phi^q_{mn}(z) e^{2\pi i(mx/L_x + ny/L_y)} \qquad (3)$$

in which m and n are the number of periods in $x-$ and $y-$direction and q is the vertical quantum number indexing various wall-normal expansions. "The direct method" (Sirovich, 1987) is used to extract the coherent structures from the Fourier transform of the two-point correlation tensor in $x-$ and $y-$direction. The expansion of the POD-modes in $z-$direction are the eigenfunctions of the integral equation

$$\int_{-1}^{1} \kappa_{ij,mn}(z,z')\phi^q_{j,mn}(z')\,dz' = \lambda^q_{mn}\phi^q_{i,mn}(z) \qquad (4)$$

in which

$$\kappa_{ij,mn}(z,z') = \frac{1}{T}\int_T \hat{u}_{i,mn}(z,t)\hat{u}^*_{j,mn}(z',t)dt \qquad (5)$$

where $\hat{u}_{i,mn}(z,t)$ is the complex Fourier coefficient of wave-number $k_x = 2\pi m/L_x$ and $k_y = 2\pi n/L_y$ in $x-$ and $y-$direction of the velocity $u_i(x,y,z,t)$. The eigenvalue problem (4) has to be solved for every combination $m,n \geq 0$. POD-modes corresponding to negative wave-numbers are found from symmetries (Sirovich, 1987).

Table 1: The 20 most energetic POD-modes of turbulent plane channel flow, $R_* = 180$.

Index	m	n	q	Lambda	d	Energy fraction
1	0	0	1	5.27E+02	1	
2	1	2	1	1.50E-02	4	8.69E-03
3	1	2	2	1.44E-02	4	8.35E-03
4	1	3	1	1.43E-02	4	8.28E-03
5	1	4	1	1.39E-02	4	8.05E-03
6	0	2	1	2.75E-02	2	7.99E-03
7	1	5	1	1.33E-02	4	7.70E-03
8	1	4	2	1.31E-02	4	7.58E-03
9	1	5	2	1.27E-02	4	7.36E-03
10	0	3	1	2.47E-02	2	7.18E-03
11	0	4	1	2.36E-02	2	6.84E-03
12	1	3	2	1.13E-02	4	6.54E-03
13	0	2	2	2.15E-02	2	6.25E-03
14	0	3	2	2.12E-02	2	6.14E-03
15	0	4	2	2.07E-02	2	5.99E-03
16	0	1	1	2.03E-02	2	5.89E-03
17	1	6	1	1.01E-02	4	5.86E-03
18	0	5	1	1.98E-02	2	5.74E-03
19	0	1	2	1.91E-02	2	5.53E-03
20	1	6	2	9.52E-03	4	5.52E-03

Now the velocity field can be expressed as

$$\boldsymbol{u}(\boldsymbol{x},t) = \sum_{mnq} a^q_{mn}(t)\boldsymbol{\varphi}^q_{mn}(\boldsymbol{x}) \qquad (6)$$

in which $\boldsymbol{\varphi}^q_{mn}(\boldsymbol{x})$ are the spatial basis functions and $a^q_{mn}(t) = \int_V \boldsymbol{u}(\boldsymbol{x},t)\cdot\boldsymbol{\varphi}(\boldsymbol{x})^{q*}_{mn}d\boldsymbol{x}$ are the temporal coefficients. In the limit of an infinite period of integration in (5), also the temporal coefficients will be orthogonal

$$\frac{1}{T}\int_T a^q_{mn}a^{r*}_{kl}\,dt = \lambda^q_{mn}\delta_{qr}\delta_{mk}\delta_{nl} \qquad (7)$$

Simpson's quadrature rule modified for stretched grid is used to approximate the integral in equation (4). Simpson's method has an error estimate of order 4.

Results from the POD. Table 1 shows the 20 most energetic modes, with corresponding λ, degeneracy, d and energy fraction of fluctuating energy. The energy in the quantum number combination (m,n,q) is defined as the energy in $\boldsymbol{\varphi}^q_{mn}$, $\boldsymbol{\varphi}^q_{-mn}$, $\boldsymbol{\varphi}^q_{m-n}$ and $\boldsymbol{\varphi}^q_{-m-n}$ (the number of degeneracies). The first mode represents the mean velocity and holds the major part of the total kinetic energy. The other modes represent fluctuating velocities. The most energy-rich modes represent elongated structures in streamwise direction.

Very Large-Eddy Simulation (VLES)

The VLES is carried out by performing a Galerkin projection of the Navier-Stokes equations on to the finite set $\mathcal{S} = \{\boldsymbol{\varphi}^q_{mn}\}$, $(m,n,q) \in \Omega$ of the eigenfunctions. Ω is the set of selected quantum number combinations. The velocity field is approximated as

$$\boldsymbol{u}(\boldsymbol{x},t) \approx \boldsymbol{u}_{\mathcal{S}} = \sum_{mnq} a^q_{mn}(t)\boldsymbol{\varphi}^q_{mn}(\boldsymbol{x}), \quad (m,n,q) \in \Omega \qquad (8)$$

The velocity $\boldsymbol{u}_{\mathcal{S}}$ is inserted into the normalised Navier-Stokes equations (1) and the inner-product with each basis function $\boldsymbol{\varphi}^q_{kl}$ in $\mathcal{S}$ is performed. The result is a system of ordinary differential equations which approximate the time evolution of the temporal coefficients, $a^q_{kl}(t)$. We follow the work of Omurtag and Sirovich (1999) who derived the dynamical system

$$\frac{d}{dt}a^q_{kl} = \sum_r \mu^{qr}_{kl} a^r_{kl} + \sum_{mnrs} \beta^{qrs}_{klmn} a^r_{mn} a^s_{k-m,l-n} + g^q \delta_{k0}\delta_{l0} \tag{9}$$

in which μ^{qr}_{kl}, β^{qrs}_{klmn} and g^q are coefficient matrixes (whose explicit expressions are not given here) depending on the eigenfunctions in $\mathcal{S}$. POD-modes representing the mean velocity (the flux modes $\{\boldsymbol{\varphi}^q_{00}\}$) are included in the set $\mathcal{S}$ leaving the system quadratic. Since the small-scale motion is not represented, an eddy-viscosity is needed to account for the effect of these on to the large-scale motion. Without any eddy-viscosity the energy level in the large-scale fluctuating modes will be too high and the mean velocity much too low. As Omurtag and Sirovich (1999) we simply add the eddy-viscosity as a constant, (e/R_*) to the molecular viscosity and e is tuned such that the bulk flow of the VLES meets the bulk flow of the DNS. Note that the eddy-viscosity is not added to the flux modes since this would imply that the mean velocity gradient $dU/dz \neq R_*$ at the wall. The boundary conditions for plane channel flow, i.e. periodicity in $x-$ and $y-$direction and no-slip condition on the walls, make the fluctuating pressure completely cancel out in the Galerkin projection. Only the predetermined mean-gradient of the pressure survives and acts as a source of energy into the flux modes $\{\boldsymbol{\varphi}^q_{00}\}$. Omurtag and Sirovich (1999) call them "mother-modes" and the remaining POD-modes feed on them.

The Simpson's quadrature rule is used to approximate the inner-product in the Galerkin projection and the system of equations (9) is integrated forward in time using a 3rd-order explicit Adams-Bashforth scheme. The derivatives of the POD-modes in $z-$direction (needed for evaluation of the coefficient matrixes) are found using a 4th-order compact scheme.

Size of the computational domain. The inlet-plane of the DNS simulation for which the inflow data are generated sets the domain length in $y-$ and $z-$direction of the VLES. Only the length in $x-$direction is a free variable. We use the length $L = L_x/3 = 4\pi H/3$ in order to keep the number of degrees of freedom in this direction at a minimum. The POD-modes were extracted from a DNS with streamwise length $L_x = 4\pi H$. In the VLES we can only include the POD-modes that are periodic at the length L, i.e. $\{\boldsymbol{\varphi}^q_{3m,n}\}$, $m,n,q = 0,\pm1,\pm2,\ldots$. The lengths in $y-$ and $z-$direction are the same as in the first DNS. A shorter length in $x-$direction implies larger jumps between the discrete wave-numbers in this direction. This again implies that the energy level (λ) of the POD-modes used in the VLES will be larger than in the DNS from which they are derived (in our case with a factor of about three). The temporal coefficient $a^q_{mn}(t)$ will from now on correspond to the extracted POD-mode $\boldsymbol{\varphi}^q_{3m,n}$.

Results from the VLES. Figures 2 and 3 show results from dynamical systems based on 4 different sets of POD-modes. The sets are $\{\boldsymbol{\varphi}^q_{3m,n}\}$ in which $m = 0,\pm1,\pm2$, $n = 0,\pm1,\ldots,\pm9$ and $q = 1,..,Q$. Q is either 2, 4, 8 or 16. For the flux modes $\{\boldsymbol{\varphi}^q_{00}\}$, Q is always equal to 32. It was found advantageous (Omurtag and Sirovich, 1999) to have a rich basis for the mean velocity. The rms-values of the normal stresses and the shear-stress are shown in figure 2 together with the DNS results. It is clear that the energy in the fluctuating streamwise component converges quicker than the two other components. The POD-modes are optimal in representing the overall energy of the flow field. Since the streamwise component contains considerably more energy than the other two components, the POD procedure puts its priority here. Figure 3 shows how the mean velocity, U, compares with the DNS. The results improve with increasing Q.

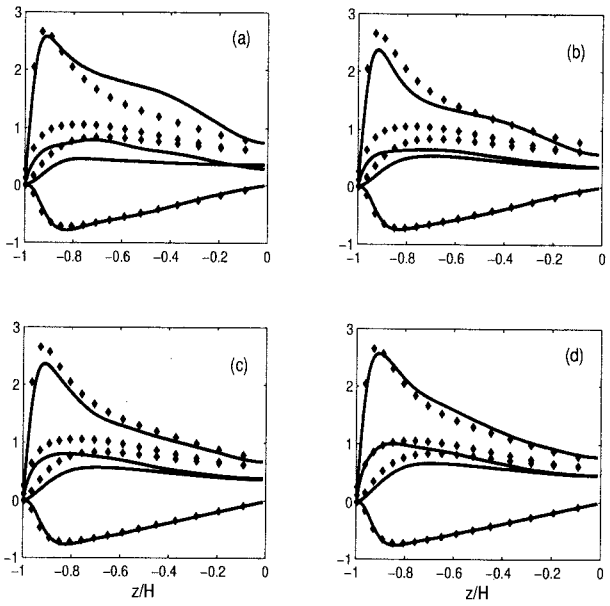

Figure 2: u-rms, v-rms, w-rms and uw $\cdots$ DNS, —— VLES (a) Q = 2, e = 2.20, (b) Q = 4, e = 1.85, (c) Q = 8, e = 1.30 and (d) Q = 16, e = 0.85

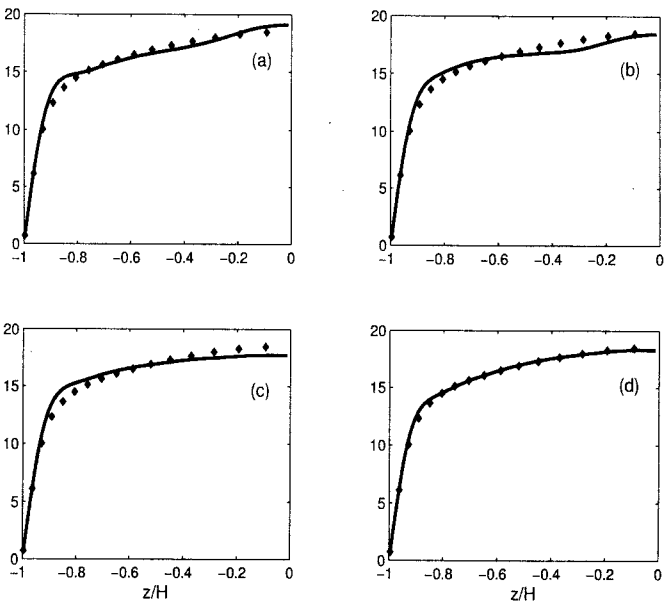

Figure 3: Mean velocity U. Legend as in figure 2

Random Small-Scale Motion

The random small-scale motion is represented as "random" POD-modes not included in the set $\mathcal{S}$. At this stage we have chosen simplicity prior to sophistication. The amplitudes of the corresponding temporal coefficients are generated by a random number generator with the distribution

$$f(x) = \frac{2}{\sqrt{2\pi}} e^{\frac{x^2}{2}}, \quad x \geq 0 \tag{10}$$

In order to impose some correlation with previous time steps we set

$$x^{new} = \frac{x^{new} + x^{old}}{2} \tag{11}$$

in which x^{new} is the random number generated at the present time step. This reduces the second moment $E(x^2)$ from 1 to ~ 0.76. The random amplitude of a^q_{mn} is set equal to $x\sqrt{3\lambda^q_{3m,n}}$. The "zero streamwise wave-number" random amplitudes a^q_{0n} correspond to very large structures in $x-$direction. We simply set the amplitude of these structures equal to zero.

The phases of temporal coefficients with nonzero streamwise wave-number behave as $\theta_0 + \omega t$ in which $\omega = -2\pi m U_{bulk}/L$ in order to imitate the propagating behaviour of these modes (Sirovich et al., 1991). The initial values θ_0 of the phases are set randomly.

The inflow velocity profiles are stored in a file which later is read by the DNS code (MGLET). The time Δt, between subsequent inflow profiles is equal to 0.01 and is larger than the viscous time scale, ($t^+ = 1/R_*$). The time step of the DNS is 0.001. In other words, we are not trying to represent the correct temporal behaviour of the small-scales at the inlet-boundary. Because of their short time-scale, it is believed that the small-scale turbulence soon will adjust to the large-scale motions.

DNS WITH GENERATED INFLOW BOUNDARY CONDITIONS

The domain size is $6\pi H$, $4\pi H/3$ and $2H$, in $x-$, $y-$ and $z-$direction, respectively. The resolution is 256 x 96 x 128 grid-points in the three directions. The resolution is somewhat increased in $x-$direction and decreased in $y-$direction in order to increase the efficiency of the multi-grid solver. Periodic boundary conditions are used in the $y-$direction. On the outflow-boundary a 3rd-order interpolation is used for the velocities. The 4th-order compact scheme is used for spatial discretization and the explicit second-order Adams-Bashforth scheme is employed for time integration. A 4th-order interpolation is used between succeeding velocity profiles at the inlet-boundary.

Two test cases are performed. The large-scale motion is produced by the same VLES and is identical in the two test cases. The set of modes used is $\mathcal{S} = \{\varphi^q_{3m,n}\}$ in which $m = 0, \pm1, \pm2$, $n = 0,...,\pm9$ and $q = 1,...,6$. For m and $n = 0$, $q = 1,...,32$. The eddy-viscosity e = 1.50. In test case 1 only the large-scale motion is introduced at the inflow boundary while in test case 2 additional small-scale random motion is superimposed. The random POD-modes consist of the set $\mathcal{N} = \mathcal{M} \setminus \mathcal{M} \cup \mathcal{S}$ where $\mathcal{M} = \{\varphi^q_{3m,n}\}$ and $m = 0,...,\pm10$, $n = 0,...,\pm40$ and $q = 1,...,15$.

Figure 4 shows the mean velocity, turbulence intensities and turbulent shear-stress imposed at the inlet in test case 1 and 2. The mean velocity is the same in both cases. For test case 2 the fluctuating energy in the streamwise component coincides with the energy of the fully developed

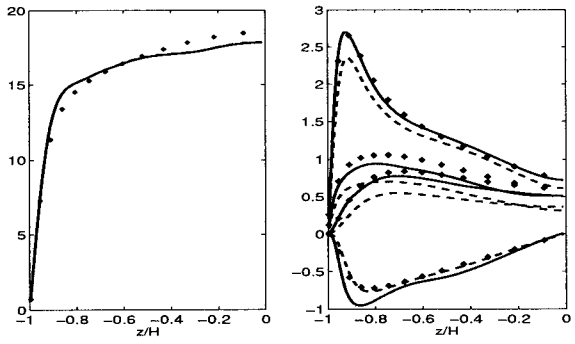

Figure 4: (left) Mean velocity, U (right) u-, v-, w-rms and $\overline{uw}$. – – – VLES, —— VLES and random motion, Symbols: DNS of fully developed channel flow.

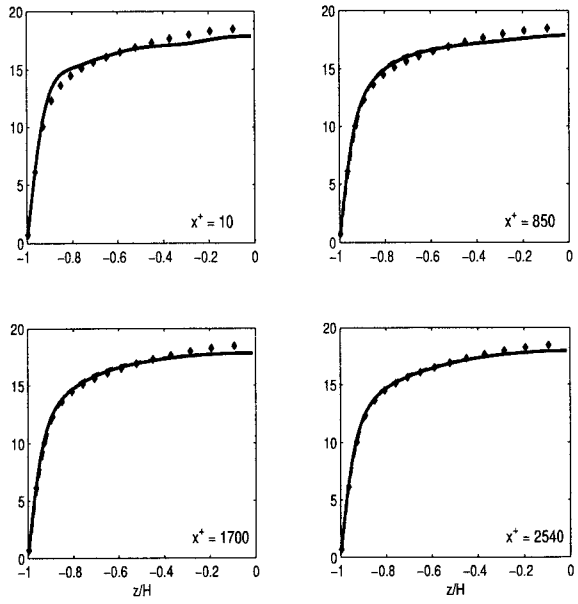

Figure 5: Mean velocity U at 4 different cross sections downstream. Legend as in figure 4.

DNS. The spanwise and wall-normal component are somewhat underestimated. The VLES adjusts itself to give the same amount of turbulent shear-stress as the DNS. Since the random POD-modes also contribute to the shear-stress, the stress level has to increase beyond the level of the DNS for test case 2.

Test Case 1 and 2

Figures 5 to 9 show how the mean velocities, turbulence intensities and turbulent shear-stress develope after the inlet for test case 1 and 2. The statistics are based on 300 samples which are averaged in the spanwise direction. The time between each sample is $0.1H/u_*$. Figure 5 shows the mean velocity. The VLES fails to predict the correct profile in the buffer region where the velocity is overestimated. In the channel centre the velocity is too low. The mean velocity has a very long time-scale and the discrepancies at the inlet-boundary are persistent and do not completely disappear in the middle of the channel even at $x^+ \approx 2500$.

In figure 6 the evolution of u-rms is presented. For test case 1 the u-rms is somewhat underestimated at inlet, but soon reach the fully developed level and beyond. The reason for this might be that the small-scale variation is not present

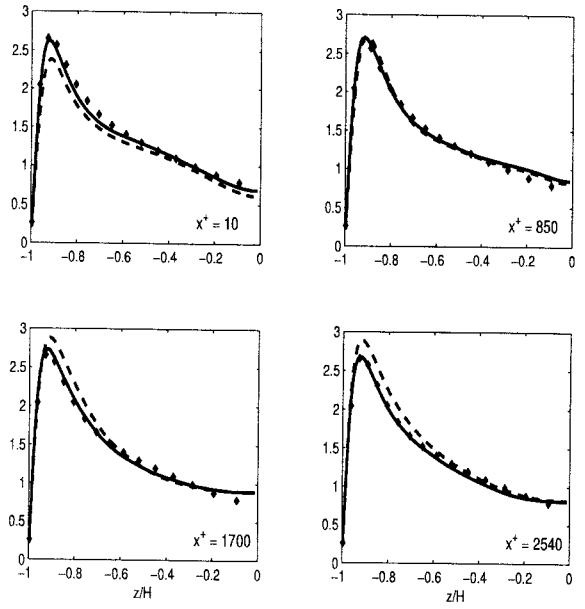

Figure 6: u-rms at 4 different cross sections downstream. – – – VLES ——, VLES and random motion, Symbols: DNS of fully developed channel flow.

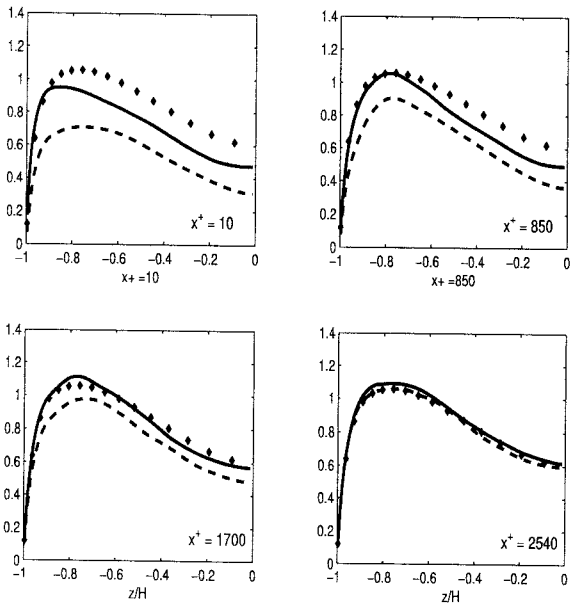

Figure 7: v-rms at 4 different cross sections downstream. Legend as in figure 6

to provide sufficient dissipation of energy. For test case 2 this is not the case and the level does not exceed the DNS except in the channel centre. The v-rms is shown in figure 7. The energy level converges smoothly towards the reference profile. Test case 2 converges faster as expected. The w-rms in figure 8 shows similar behaviour as the v-rms.

The turbulent shear-stress in figure 9 behaves less satisfactorily. The correlation seems to decay to some degree after the inlet. The decay is more appearent in test case 1 than in test case 2. At $x^+ \approx 2500$ the shear-stress profiles are the same for test case 1 and 2, but has not completely recovered within this length. The shear-stress profile is of course connected to the mean velocity profile. The shear-stress gradient is larger in the buffer region and smaller in

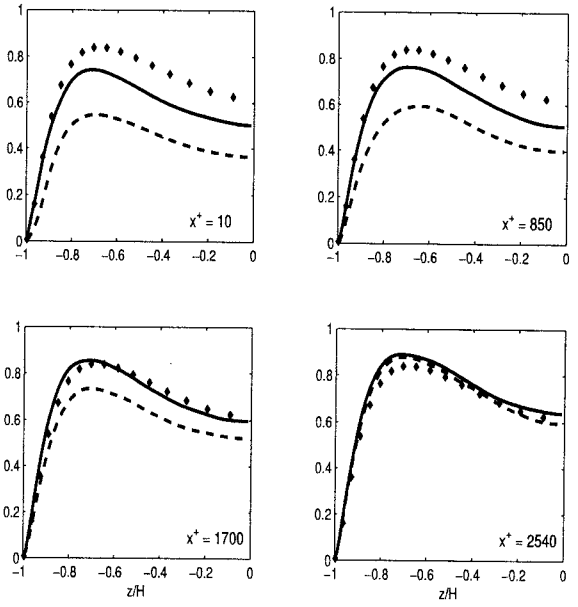

Figure 8: w-rms at 4 different cross sections downstream. Legend as in figure 6

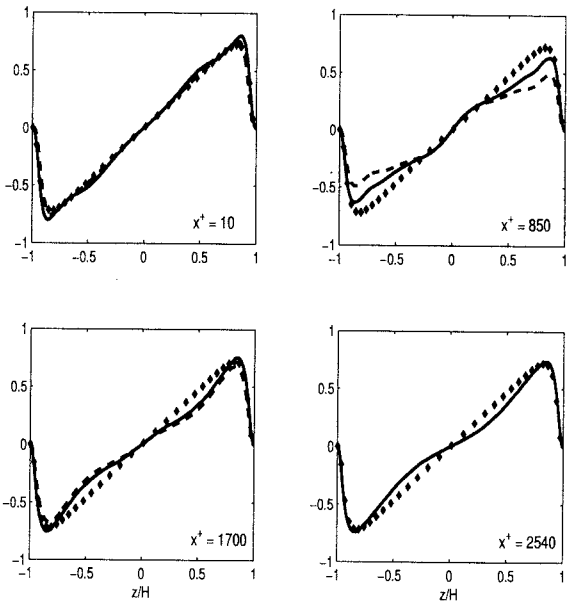

Figure 9: Turbulent shear-stress at 4 different cross sections downstream. Legend as in figure 6

the channel centre than for the fully developed DNS indicating that the channel core is accelerating.

Figure 10 and figure 11 show the Fourier transform of the one-dimensional spanwise correlations R_{uu} and R_{ww}, respectively. The correlations are averaged along lines placed at 100 wall units from the wall and at 4 different locations downstream. All three spectra (E_{vv} is not shown) behave qualitatively in the same manner. In the first plane just after the inlet there is a sharp drop in the spectra for test case 1 corresponding to the maximum spanwise wave-number in the VLES. The energy is not completely zero in the high wave-number part of the spectrum as it theoretically should be. A plausible explanation for this is the interpolation of the POD-modes on to the staggered grid positions used by the finite volume code. In test case 2 this part of the

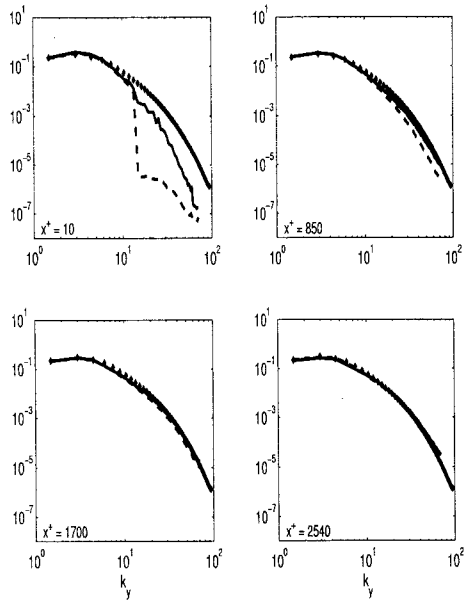

Figure 10: One-dimensional energy spectra, E_{uu}, at 4 different cross sections downstream the inlet: – – –; Test case 1, ——; Test case 2, Symbols; fully developed channel flow

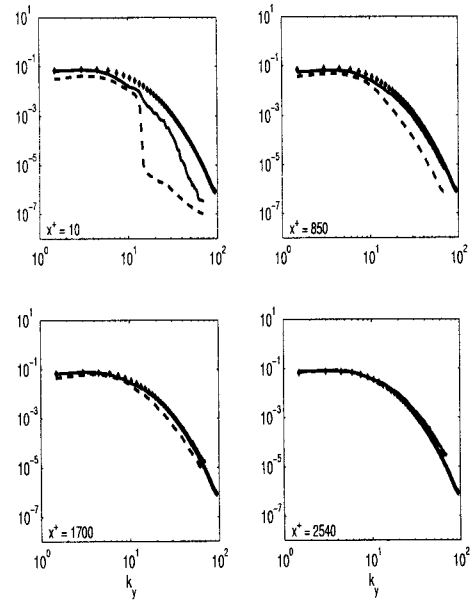

Figure 11: One-dimensional energy spectra, E_{ww}, at 4 different cross-sections downstream the inlet. Legend as in figure 10

spectrum is generated randomly, but the energy level is underestimated as only a subset of the total set of POD-modes is randomly varied. Test case 2 spectra develop faster towards the spectra of the fully developed flow than the spectra of test case 1.

CONCLUDING REMARKS

This study suggest that turbulence produced by a low-dimensional dynamical system based on POD-modes can be appropriate as turbulent inlet-boundary conditions. It seems advantageous to superimpose low energy random POD-modes on to the large-scale motion produced by the VLES in order to introduce some energy in the high wave-number region and sooner initiate the correct level of dissipation. For engineering problems it is suggested that for a Reynolds number about 180 an entrance region of 1000 wall units should be sufficient. At this point the turbulence will not be far from fully developed, at least in terms of one-point second-order statistics and energy spectra. If fully developed turbulence is needed for rigorous scientific studies the proposed procedure is unable to compete with the running of a separate DNS with periodic boundary conditions, especially since such a simulation enables use of the direct solver. The inconvenience with the rather long time needed to arrive at a fully developed stage from random and unphysical disturbances can be partially eliminated in combination with the procedure suggested here since the same approach can be used to produce "good" start-fields. The time needed for the dynamical systems studied here to arrive at "fully developed" state is negligible.

It still remains to verify if the POD-modes from one Reynolds number can be used as basis for a VLES at another Reynolds number and how these dynamical systems behave when the POD-modes are stretched to fit another aspect ratio of the channel. These are important issues to shed light upon in order to settle if this can be a method to cheaply generate turbulent inlet velocities for a fairly general plane channel flow.

ACKNOWLEDGEMENT

The first author was the recipient of a research fellowship offered by the Research Council of Norway. We also acknowledge The Research Council of Norway (Programme for Supercomputing) for granting us necessary CPU time. The MGLET code was generously made available by Prof. H. Wengle (Universität der Bundeswehr München) and Prof. R. Friedrich (Technische Universität München). Valuable discussions with Prof. E.M. Rønquist (Trondheim) are highly appreciated.

REFERENCES

Holmes,P., Lumley J.L. and Berkooz G. (1996), "Turbulence, Coherent Structures, Dynamical Systems and Symmetry", Cambridge University Press, Cambridge

Kim J., Moin P. and Moser R. (1987), "Turbulence statistics in fully developed channel flow at low Reynolds number", *J. Fluid Mech.*, Vol. 177, pp 133-166.

Lumley J.L. (1967), "The structure of inhomogeneous turbulence", *Atmospheric Turbulence and Wave Propagation* A. M. Yaglom and V.I. Tatarski, ed., Nauka, Moscow

Lygren M. and Andersson H.I. (2001), "Turbulent flow between a rotating and stationary disk", *J. Fluid Mech.* Vol. 426, pp 297-326

Manhart M. and Wengle H. (1993) "A spatiotemporal decomposition of a fully inhomogeneous turbulent flow field", *Theoret. Comput. Fluid Dynamics*, Vol.5, pp 223-242

Omurtag A. and Sirovich L. (1999) "On low-dimensional modeling of channel turbulence", *Theoret. Comput. Fluid Dynamics* Vol.13, pp 115-127

Sirovich L. (1987) "Turbulence and the dynamics of coherent structures, Parts i-iii", *Quarterly of Applied Mathematics*, Vol.45, pp 561-591

Sirovich L., Ball K.S. and Handler R.A. (1991) "Propagating structures in wall-bounded turbulent flows" *Theoret. Comput. Fluid Dynamics* Vol. 2, pp 307-317